Research Article

NMR IN BIOMEDICINE

Received: 10 August 2010, Revised: 24 November 2010, Accepted: 14 December 2010, Published online in Wiley Online Library: 15 March 2011

(wileyonlinelibrary.com) DOI:10.1002/nbm.1677

A lanthanide complex with dual biosensing properties: CEST (chemical exchange saturation transfer) and BIRDS (biosensor imaging of redundant deviation in shifts) with europium DOTA–tetraglycinate

Daniel Coman[a,b,c]*, Garry E. Kiefer[d], Douglas L. Rothman[a,b,c,e], A. Dean Sherry[f,g] and Fahmeed Hyder[a,b,c,e]*

Responsive contrast agents (RCAs) composed of lanthanide(III) ion (Ln^{3+}) complexes with a variety of 1,4,7,10-tetraazacyclododecane-1,4,7,10-tetraacetate ($DOTA^{4-}$) derivatives have shown great potential as molecular imaging agents for MR. A variety of LnDOTA–tetraamide complexes have been demonstrated as RCAs for molecular imaging using chemical exchange saturation transfer (CEST). The CEST method detects proton exchange between bulk water and any exchangeable sites on the ligand itself or an inner sphere of bound water that is shifted by a paramagnetic Ln^{3+} ion bound in the core of the macrocycle. It has also been shown that molecular imaging is possible when the RCA itself is observed (i.e. not its effect on bulk water) using a method called biosensor imaging of redundant deviation in shifts (BIRDS). The BIRDS method utilizes redundant information stored in the nonexchangeable proton resonances emanating from the paramagnetic RCA for ambient factors such as temperature and/or pH. Thus, CEST and BIRDS rely on exchangeable and nonexchangeable protons, respectively, for biosensing. We posited that it would be feasible to combine these two biosensing features into the same RCA (i.e. dual CEST and BIRDS properties). A complex between europium(III) ion (Eu^{3+}) and DOTA–tetraglycinate [DOTA–$(gly)_4^-$] was used to demonstrate that its CEST characteristics are preserved, while its BIRDS properties are also detectable. The *in vitro* temperature sensitivity of EuDOTA–$(gly)_4^-$ was used to show that qualitative MR contrast with CEST can be calibrated using quantitative MR mapping with BIRDS, thereby enabling quantitative molecular imaging at high spatial resolution. Copyright © 2011 John Wiley & Sons, Ltd.

Keywords: amide protons; DIACEST; hydroxyl protons; methyl protons; PARACEST; pH; temperature

INTRODUCTION

Paramagnetic complexes are widely used as MRI contrast agents in clinical medicine. These agents—many of which are composed of a lanthanide(III) ion (Ln^{3+}) with a 1,4,7,10-tetraazacyclododecane-1,4,7,10-tetraacetate ($DOTA^{4-}$) backbone—generate contrast by affecting the bulk water proton relaxation rate. However, this approach often lacks sensitivity

* *Correspondence to: F. Hyder, D. Coman, N135 TAC (MRRC), 300 Cedar Street, Yale University, New Haven, CT 06520, USA. E-mail: fahmeed.hyder@yale.edu, daniel.coman@yale.edu*

a *D. Coman, D. L. Rothman, F. Hyder*
Magnetic Resonance Research Center (MRRC), Yale University, New Haven, CT, USA

b *D. Coman, D. L. Rothman, F. Hyder*
Core Center for Quantitative Neuroscience with Magnetic Resonance (QNMR), Yale University, New Haven, CT, USA

c *D. Coman, D. L. Rothman, F. Hyder*
Department of Diagnostic Radiology, Yale University, New Haven, CT, USA

d *G. E. Kiefer*
Macrocyclics, Dallas, TX, USA

e *D. L. Rothman, F. Hyder*
Department of Biomedical Engineering, Yale University, New Haven, CT, USA

f *A. D. Sherry*
Advanced Imaging Research Center and Department of Radiology, University of Texas Southwestern Medical Center, Dallas, TX, USA

g *A. D. Sherry*
Department of Chemistry, University of Texas, Dallas, TX, USA

Abbreviations used: *BIRDS, biosensor imaging of redundant deviation in shifts; CEST, chemical exchange saturation transfer; COSY, correlation spectroscopy; CSI, chemical shift imaging; DIACEST, diamagnetic CEST; $DOTA^{4-}$, 1,4,7,10-tetraazacyclododecane-1,4,7,10-tetraacetate; DOTA–$(gly)_4^-$, DOTA–tetraglycinate; $DOTMA^{4-}$, 1,4,7,10-tetramethyl-1,4,7,10-tetraazacyclododecane-1,4,7,10-tetraacetate; $DOTP^{8-}$, 1,4,7,10-tetraazacyclododecane-1,4,7,10-tetrakis(methylene phosphonate); PARACEST, paramagnetic CEST; RCA, responsive contrast agent; RF, radiofrequency; SNR, signal-to-noise ratio.*

and/or specificity for tracking diseases as the contrast is always 'on' when the agent is present. The imaging of specific ions or metabolites is becoming possible with MRI probes, either endogenous or exogenous, which contain exchangeable protons (1,2). The chemical exchange saturation transfer (CEST) technique detects exchange between bulk water protons and amide (i.e. $-NH_x$ where $x = 1$ or 2) or hydroxyl (i.e. $-OH$) protons in diamagnetic molecules, whereas, in paramagnetic molecules, the exchangeable pool is either any exchangeable sites on the ligand itself or protons in an inner sphere of bound water that is significantly shifted by Ln^{3+} in the agent's core. The CEST method has tremendous translational potential because it amplifies the detection of extracellular targets present at the micromolar to millimolar level. A great appeal for biomedical imaging is that CEST contrast, with either diamagnetic or paramagnetic agents, can be switched 'on' or 'off' with a radiofrequency (RF) saturation pulse.

From the earliest days of MRS, exchange between bulk solvent water protons (10^1–10^2 M) and bound solute protons (10^{-3}–10^{-2} M) has been studied using saturation transfer techniques [see ref. (3) for details]. CEST with endogenous diamagnetic molecules (e.g. sugars or proteins) is now commonly called DIACEST. Because the chemical shift of a typical diamagnetic exchangeable proton is within a few parts per million of bulk water protons, off-resonance direct saturation of bulk water, indirect saturation via water tightly bound to macromolecules and poor static magnetic field (B_0) homogeneity are matters that complicate *in vivo* DIACEST imaging. To help circumvent these problems, a class of paramagnetic CEST probes consisting of Ln^{3+} bound in a DOTA–tetraamide core, called PARACEST agents, have been synthesized to increase the chemical shift separation ($>10^n$ ppm, where $n \geq 1$) between the signals arising from a pool of exchangeable protons of an inner sphere of bound water and bulk solvent water (4,5). This approach allows the tuning of water exchange kinetics by the choice of chelate structure and/or Ln^{3+} to improve CEST contrast (2,6). Some PARACEST agents contain bound water molecules with a lifetime in the microseconds range (7). To date, exogenous PARACEST agents have been used to measure various physiological parameters, e.g. pH (5), temperature (8,9), lactate (10) and glucose (11,12). Moreover, the quantification of physiologically relevant metal ions, e.g. calcium (13) and zinc (14), has been achieved by relaxivity changes of these types of agents. Furthermore, preliminary toxicity studies of prototypical PARACEST agents have shown them to be chemically inert in animals, so that moving these towards clinical approval is quite conceivable in the near future (15).

Various PARACEST-like agents have been characterized beyond their effects on the bulk water relaxation rate or proton exchange. Many have been differentiated in terms of their structure, conformation and relaxation properties (16,17), thermodynamics, protonation and coordination to alkali metals (18), stability, biodistribution and toxicity (19), as well as sensitivities of nonexchangeable nuclei to ambient factors such as temperature and/or pH (20). Previous attempts at the biosensing of temperature and/or pH in animal brain by direct detection of Ln^{3+}-based agents may have failed (21) because of very low B_0, poor gradient performance and/or unfamiliarity with the agent's relaxation properties. More recently, with modern technology, these factors have been overcome, enabling the biosensing of temperature and/or pH (22) using a technique termed biosensor imaging of redundant deviation in shifts (BIRDS) (23,24). The BIRDS method utilizes the redundant information stored in chemical shifts emanating from the paramagnetic Ln^{3+}-based agent for ambient factors such as temperature and/or pH. To date, mainly the agent's nonexchangeable proton resonances (i.e. $-CH_x$) have been measured, but all other observable nuclei (^{17}O, ^{15}N, ^{13}C, ^{31}P) are equally viable candidates for BIRDS. Superior temperature and/or pH sensitivities of proton chemical shifts emanating from two thulium(III) ion (Tm^{3+})-containing macrocyclics [1,4,7,10-tetraazacyclododecane-1,4,7,10-tetrakis (methylene phosphonate) (or $DOTP^{8-}$) and 1,4,7,10-tetramethyl-1,4,7,10-tetraazacyclododecane-1,4,7,10-tetraacetate (or $DOTMA^{4-}$)] have been demonstrated in rat brain with BIRDS (23,24). Generally, agents with BIRDS properties stand in contrast with PARACEST agents by the fact that, in the latter, only the effect on bulk water is detected, whereas, in the former, the agent itself is detected. This enables BIRDS to be more quantitative than CEST, but with a much lower spatial resolution. As the relative advantages and disadvantages of BIRDS and CEST do not apparently overlap, it is tantalizing to consider a new family of agents that could combines these two sets of properties.

As CEST and BIRDS methods differ by their dependence on exchangeable and nonexchangeable protons, respectively, for biosensing, we conjectured whether these two features could be supported on the same agent for improved biosensing with dual CEST and BIRDS properties. To test this, we chose a complex between the europium(III) ion (Eu^{3+}) and a tetraglycinate derivative of $DOTA^{4-}$, EuDOTA–$(gly)_4^-$, which has been characterized previously as a PARACEST agent (5,7) for temperature sensing (9). *In vitro* results were used to corroborate that CEST attributes are fully conserved, whereas BIRDS properties are detected, to enable the possibility that qualitative MR contrast with CEST could be calibrated using quantitative MR mapping with BIRDS. These types of agents with dual CEST and BIRDS properties provide an opportunity for quantitative molecular imaging at high spatial resolution.

MATERIALS AND METHODS

BIRDS experiments with EuDOTA–$(gly)_4^-$

To assess the BIRDS properties of EuDOTA–$(gly)_4^-$, a database composed of ^1H spectra as a function of temperature was compiled by studying samples of EuDOTA–$(gly)_4^-$ (5 mM) at different pH values (pH 6.5–8.0) in phosphate buffer (5 mM). The ^1H MRS data of EuDOTA–$(gly)_4^-$ were acquired on an 11.7-T Bruker (Billerica, MA, USA) vertical-bore spectrometer at temperatures between 26 and 40 °C using a recycle time (TR) suitable for short relaxation times of these types of agent (Fig. 1A). The correct temperature calibration of the RF probe's thermocouple was verified by two additional methods. The first method was based on the chemical shift difference between the $-OH$ and $-CH_3$ resonances of deuterated methanol (Sigma-Aldrich, St. Louis, MO, USA, No. 343803-5G) (25). For the second method, a thermocouple wire was immersed directly into the solution of the NMR tube. The temperatures measured by both methods in the 26–40 °C range were within ±0.5% of the temperature indicated by the probe's thermocouple. The small fluctuation in the values of the measured temperatures is probably a result of inherent errors associated with each temperature measurement technique. For the deuterated methanol method, propagation of errors shows that a 1-Hz error in the measurement of the chemical shift difference results in a 0.2 °C error in temperature. Moreover,

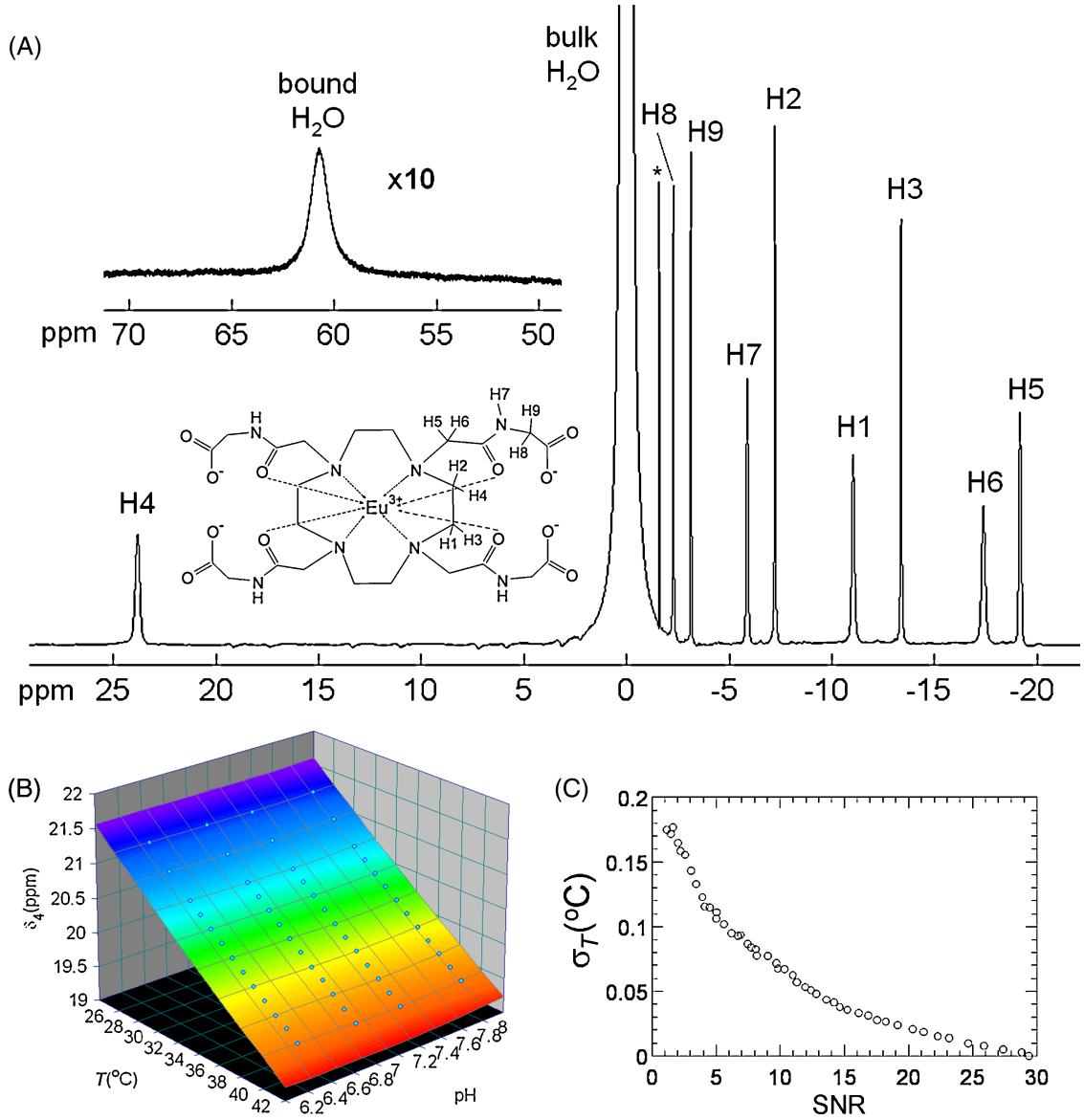

Figure 1. BIRDS (biosensor imaging of redundant deviation in shifts) characterization of europium DOTA–tetraglycinate [EuDOTA–$(gly)_4^-$] ($DOTA^{4-}$, 1,4,7,10-tetraazacyclododecane-1,4,7,10-tetraacetate). (A) Proton spectrum at pH 7.0 and 10 °C. Insets represent the chemical structure of EuDOTA–$(gly)_4^-$ and the bound water resonance at ~60 ppm. The ^{1}H resonances were assigned by two-dimensional correlation spectroscopy (COSY). The resonance marked by '*' corresponds to traces of a high-performance liquid chromatography solvent left in the sample after purification. The H7 proton belongs to the amide. (B) Three-dimensional surface plot showing the temperature and pH dependence of the H4 proton chemical shift, which is unaffected by pH, thereby simplifying the equation for temperature calibration to a second-order polynomial (Equation [1]). (C) Accuracy of temperature determination at various signal-to-noise ratios (SNRs) for the H4 resonance. The SNR of a voxel during a typical *in vitro* chemical shift imaging (CSI) experiment is in the range 10–25, which corresponds to a standard deviation in temperature of 0.07 °C or smaller.

deviation from Lorentzian lineshapes of both $-OH$ and $-CH_3$ resonances of deuterated methanol, albeit with good shimming at the different temperatures measured, suggests the existence of temperature gradients within the sample, probably as a result of nonuniform heating/cooling processes. The existence of this temperature gradient could also contribute to the measured temperature for the thermocouple method. The pH in each sample was measured by a (Corning, NY, USA) 430 pH-meter with a Beckman (Fullerton, CA, USA) glass electrode ($5 \times 178\,mm^2$, Calomel). The spectra of EuDOTA–$(gly)_4^-$, were line broadened (10 Hz) and then baseline (first-order) and phase (zero-order) corrected. The assignments for proton resonances were obtained by a two-dimensional correlation spectroscopy (COSY) experiment. The chemical shifts were measured after each resonance was fitted to a Lorentzian lineshape. Longitudinal (T_1) and transverse (T_2) relaxation times of each proton were measured at 35 °C using conventional inversion recovery and spin-echo methods, respectively. T_1 and T_2 values were obtained by fitting the time-dependent intensities to a single exponential. For the temperature calibration with EuDOTA–$(gly)_4^-$, the most sensitive nonexchangeable proton was chosen and the absolute temperature T_c was calculated using the variation in the chemical shift δ_x according to:

$$T_c = a_0 + a_1(\delta_x - \delta_0) + a_2(\delta_x - \delta_0)^2 \quad [1]$$

where δ_0 was set to 20.0 ppm and the coefficients a_0, a_1 and a_2 were determined from a linear least-squares fit of the measured

temperature as a function of the chemical shift. The calculated temperature values T_c from Equation [1] were later compared with independently measured temperature values T_m using a thermocouple wire located around the RF coil, reflecting the sample's temperature (see Equation [4]).

The effect of the signal-to-noise ratio (SNR) of the resonance on the temperature determination was assessed by the addition of uniformly distributed random noise of varying amplitudes to the original free induction decay prior to Fourier transformation (23). Baseline (first-order) and phase (zero-order) corrections were applied to the spectrum and the peak of interest was fitted to a Lorentzian lineshape. The SNR was calculated from the 'signal' and 'noise' values using the equation (26):

$$\mathrm{SNR} = 20 \times \log_{10}\left(\frac{\mathrm{signal}}{\mathrm{noise}}\right) \quad [2]$$

where the 'signal' was given by the height of the resonance and the 'noise' was estimated from the standard deviation of the signal in a region away from any resonance. For each noise amplitude, 100 different runs were used to estimate the corresponding average SNR value and to measure the H4 chemical shifts. Using these chemical shifts, the corresponding temperatures were calculated using Equation [1]. The standard deviation in temperature σ_T was estimated for each SNR value from the temperature values obtained during each of the 100 runs.

CEST experiments with EuDOTA–(gly)$_4^-$

CEST properties are based on the acquisition of *Z* spectra, which are frequency-dependent saturation spectra (27,28). The ratio M/M_0, which represents the intensity of the bulk water resonances at a certain saturation frequency (i.e. M with RF saturation 'on') *versus* the intensity of the bulk water with the saturation frequency at −100 ppm (i.e. M_0 with RF saturation 'off'), was plotted against the frequency of the RF saturation pulse to obtain the *Z* spectra. Thus, at each frequency of the RF saturation pulse applied, the fractional decrease in the intensity of the bulk water signal was reported, where the intensity of the signal was given by the amplitude of the bulk water resonance. All *Z* spectra were acquired on the same 11.7-T Bruker vertical-bore spectrometer as the data acquired for BIRDS. The samples contained EuDOTA–(gly)$_4^-$ (5–50 mM) and 10% D_2O. A continuous-wave RF irradiation of 1 s was used for the saturation of various frequencies to obtain the *Z* spectra. For the temperature dependence, a sample of 5 mM EuDOTA–(gly)$_4^-$ at pH 7.42 was used and the temperature was varied between 25 and 40 °C. For the pH dependence, samples of 5 mM EuDOTA–(gly)$_4^-$ at 30 °C were used with the pH in the range 6.5–8.0. For the agent concentration dependence, samples at 30 °C were used with EuDOTA–(gly)$_4^-$ concentrations in the range 5–50 mM. For the TR dependence, a sample of 10 mM EuDOTA–(gly)$_4^-$ at pH 7.0 at 30 °C was used and TR was varied from 1 to 10 s, with the presaturation pulse of 1 s maintained constant. Each ^{1}H spectrum was line broadened (5 Hz), and baseline (first-order) and phase (zero-order) corrected. The intensity of the bulk water resonance was measured at each RF saturation frequency to generate the Z spectra.

Combined CEST and BIRDS experiments with EuDOTA–(gly)$_4^-$

The phantom used for *in vitro* imaging experiments consisted of a glass tube containing 20 mM of EuDOTA–(gly)$_4^-$ in 10% D_2O at pH 7.0. The CEST data were acquired in ^{1}H MRI format, whereas the ^{1}H MRS data for BIRDS were acquired in two-dimensional chemical shift imaging (CSI) format. The CSI and MRI data, of similar slice position (sample center) and width (2 mm), were acquired on a modified 11.7-T Bruker horizontal-bore spectrometer using a ^{1}H surface coil RF probe (diameter, 1.4 cm). The ambient temperature was controlled using a water-heating blanket wrapped around the phantom, but positioned such that enough space (1–2 cm) was left between the phantom and the blanket. The phantom's temperature was measured by a thermocouple wire (diameter, ~100 μm; copper-constantan; ± 0.05 °C; Oxford Optronix, Oxford, UK) positioned at the bottom.

For CSI experiments, a field of view of 2.56 × 2.56 cm^2 was used with 32 × 32 phase-encoding steps. A 1-ms Gaussian excitation pulse was used for selective excitation of the most sensitive nonexchangeable proton resonance. The phase-encode gradient duration was 100 μs and TR was 60 ms. Two different CSI datasets were obtained. One at room temperature (~ 22 °C) with the water bath turned off, and the second with the water bath temperature at 60 °C which resulted in an ambient temperature around the sample of approximately 42 °C. The spectra were processed as described above for the temperature calibration experiments.

The MRI experiments were acquired using a spin-echo imaging sequence. The imaging parameters were TR = 6 s, TE = 10 ms, field of view of 16 × 16 mm^2 and image matrix of 128 × 128. A 1-s square pulse was used for presaturation of the bound water prior to the beginning of the spin-echo sequence. At each ambient temperature, two images were acquired, one with the saturation offset at the frequency of the bound water resonance (24 kHz, 'on' saturation) and the other with the saturation offset on the opposite side of the bulk water resonance (−24 kHz, 'off' saturation). We used a single saturation frequency of 24 kHz for both temperatures because the bound water peak is very broad, with linewidths much larger than the temperature-induced shift of the water bound peak. Moreover, the use of a single saturation frequency bypasses the requirement of measuring the position of the bound water peak before each imaging experiment. For each voxel, the fractional decrease in the intensity of the bulk water signal M was reported according to:

$$M = 1 - \frac{M_{\mathrm{on}}}{M_{\mathrm{off}}} \quad [3]$$

where M_{on} and M_{off} represent the bulk water intensities for the 'on' and 'off' saturation experiments, respectively.

RESULTS

Characterization of EuDOTA–(gly)$_4^-$ with BIRDS

A ^{1}H spectrum of EuDOTA–(gly)$_4^-$ (Fig. 1A) shows that its resonances span a relatively wide chemical shift range of approximately 40 ppm, although this range is far less wide than that of other Tm^{3+}-based agents, such as $TmDOTP^{5-}$ and $TmDOTMA^-$ (23,24). Each ^{1}H resonance, exchangeable or not, was assigned on the basis of the two-dimensional COSY experimental result (data not shown). There are two exchangeable protons observed with EuDOTA–(gly)$_4^-$. First, the bound water signal, better visualized at a lower temperature of approximately 10 °C or so, is located at approximately 60 ppm from bulk water (Fig. 1A, inset spectrum). Second, the H7 proton belongs to an amide group (Fig. 1A, inset structure). The remaining protons are all nonexchangeable with variable

Table 1. Temperature sensitivities and relaxation times for europium DOTA–tetraglycinate [EuDOTA–$(gly)_4^-$] protons (at 35 °C and pH 7.0)

Proton	Temperature sensitivity (ppm/ °C)	T_1 (ms)	T_2 (ms)
H1	0.0593 ± 0.0002	30.9 ± 1.2	5.6 ± 0.3
H2	0.0051 ± 0.0003	38.7 ± 1.3	6.3 ± 0.3
H3	0.0223 ± 0.0003	34.9 ± 0.6	7.0 ± 0.3
H4	-0.1299 ± 0.0003	26.7 ± 1.3	6.2 ± 0.2
H5	0.0754 ± 0.0004	37.1 ± 1.7	7.0 ± 0.5
H6	0.1033 ± 0.0004	29.0 ± 1.0	5.8 ± 0.2
H7[a]	–	–	–
H8	0.0154 ± 0.0004	140.5 ± 5.1	10.2 ± 0.9
H9	0.0242 ± 0.0005	151.6 ± 3.2	6.1 ± 0.5

$DOTA^{4-}$, 1,4,7,10-tetraazacyclododecane-1,4,7,10-tetraacetate.
[a]The H7 amide proton is in fast exchange with the bulk water (observed at temperatures of 15 °C).

degrees of sensitivity to temperature and relaxation times (Table 1). Although several nonexchangeable protons show variable degrees of temperature sensitivity without any noteworthy pH dependence, the H4 proton has the highest temperature sensitivity and good separation from other resonances (Fig. 1A). The linewidths of the EuDOTA–$(gly)_4^-$ protons, at 35 °C and pH 7.42, are 50–70 Hz, with the H4 proton resonance having the largest value. Under these conditions, the temperature sensitivities of the EuDOTA–$(gly)_4^-$ protons are in the range 0.005–0.13 ppm/ °C, where, again, the H4 proton has the highest value. These data point to the use of the H4 proton to provide the early temperature characterization of EuDOTA–$(gly)_4^-$ with BIRDS. Thus, the absolute temperature T_c was calculated from the chemical shift of the H4 proton signal as δ_x in Equation [1] using fitted values of the coefficients a_0, a_1 and a_2 (Table 2).

Using error propagation (29), it can be shown that the uncertainties in temperature (ε_T) are proportional to the chemical shift uncertainties (ε_δ): $\varepsilon_T = 7.74 \times \varepsilon_\delta$. A very high correlation coefficient ($R = 0.99998$) between the calculated temperature T_c and the thermocouple measured temperature T_m was obtained by linear least-squares fitting, as shown by the following linear equation with an intercept close to zero and a slope of unity:

$$T_c = (-0.01 \pm 0.06) + (1.000 \pm 0.002)T_m \quad [4]$$

To verify the accuracy of the temperature determination, as described by Equation [4], we employed an alternative cross-validation method, the 'leave one out' method. In this method, the temperature calibration described by Equation [1] was performed using a dataset without one of the temperature–chemical shift data points. This data point was then used to evaluate the accuracy of the method by calculating the temperature corresponding to the chemical shift data point not used for calibration. The same procedure was repeated for each data point and the correlation between the calculated temperature using the 'leave one out' method, $T_c^{(1out)}$, and the measured temperature T_m was determined:

$$T_c^{(1out)} = (-0.02 \pm 0.08) + (1.001 \pm 0.002)T_m \quad [5]$$

As Equations [4] and [5] are very similar (i.e. each with a very high correlation coefficient, an intercept close to zero and a slope of unity), these results indicate that EuDOTA–$(gly)_4^-$ is a very good temperature probe for BIRDS. At 11.7 T, for a 5-mM sample of EuDOTA–$(gly)_4^-$ at 35 °C and pH 7.0, all of the nonexchangeable protons have T_1 and T_2 values in the range 30–150 ms and 5–10 ms, respectively (Table 1). This indicates that a short TR can be used for the two-dimensional CSI data acquisition needed for BIRDS.

Repeated simulations of temperature determination using the H4 chemical shift (Equation [1]), but with different SNR, were used to address the question of how the error of temperature measurement (σ_T) depends on SNR (23). The error of the temperature prediction was estimated by means of the temperature standard deviations for 100 runs at a given SNR value (Fig. 1C). Typical *in vitro* SNR values for the H4 proton are in the range of 10–30 for a voxel of $0.8 \times 0.8 \times 2\,mm^3$. This SNR range corresponds to a temperature standard deviation of less than 0.07 °C (Fig. 1C). Similar standard deviations in temperature (0.06 °C) were obtained using the *N*-acetyl aspartate and water method, but for a much larger voxel size of $1.6 \times 1.6 \times 4\,mm^3$ (23). Therefore, EuDOTA–$(gly)_4^-$ with BIRDS is at least as good as the *N*-acetyl aspartate–water method for temperature determination, with the potential of a considerably higher spatial resolution (23,24). The temperature accuracy (by BIRDS) as a function of SNR has been estimated previously for two other Tm^{3+}-based agents: $TmDOTP^{5-}$ and $TmDOTMA^-$ (23,24). The temperature standard deviations in a spectrum of a CSI voxel, acquired under identical experimental conditions (i.e. volume, acquisition time, agent concentration), were 0.01 °C for EuDOTA–$(gly)_4^-$ at SNR = 25 (Fig. 1C) and 0.008 and 0.002 °C for $TmDOTP^{5-}$ and $TmDOTMA^-$, respectively (23). Thus, the accuracy of temperature determination with EuDOTA–$(gly)_4^-$ is comparable with that with $TmDOTP^{5-}$, but slightly lower than that with $TmDOTMA^-$.

Table 2. Coefficients a_0, a_1 and a_2 for temperature with H4 resonance of europium DOTA–tetraglycinate [EuDOTA–$(gly)_4^-$]

Coefficient	Value
a_0	35.30 ± 0.01
a_1	-7.74 ± 0.02
a_2	0.32 ± 0.02

$DOTA^{4-}$, 1,4,7,10-tetraazacyclododecane-1,4,7,10-tetraacetate.

Characterization of EuDOTA–$(gly)_4^-$ with CEST

As it is well known that CEST contrast depends on many experimental factors (e.g. B_0 inhomogeneity, temperature and/or pH around the agent, agent concentration, TR of CEST experiment, etc.) (1,2), we acquired *Z* spectra of EuDOTA–$(gly)_4^-$ under various experimental conditions to characterize its CEST properties (Fig. 2). EuDOTA–$(gly)_4^-$ is a well-known PARACEST agent for temperature mapping (5,7,9). The CEST effect from the exchangeable water molecule increases with increasing temperature (Fig. 2A). CEST is more efficient at higher temperatures because the exchange of water molecules between the two pools is faster. Above approximately 40 °C, however, the CEST effect begins to decline once again because water exchange becomes

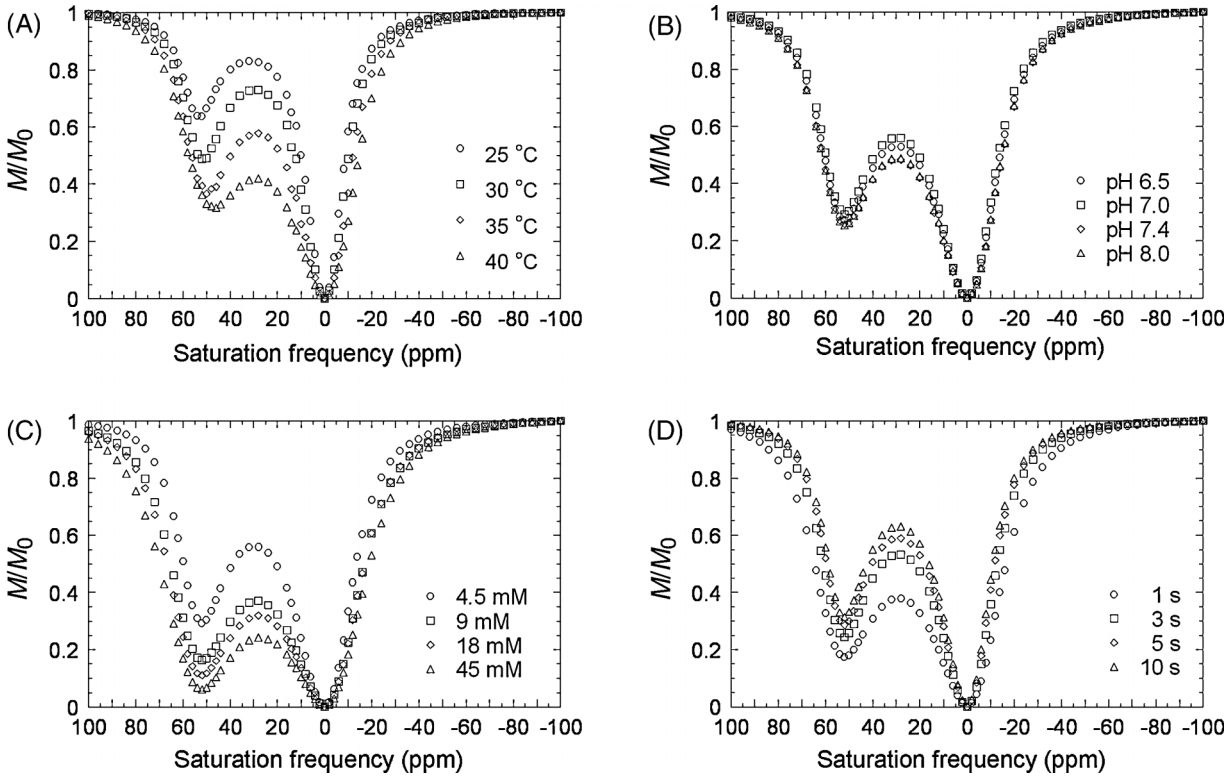

Figure 2. Chemical exchange saturation transfer (CEST) characterization of europium DOTA–tetraglycinate [EuDOTA–$(gly)_4^-$] ($DOTA^{4-}$, 1,4,7,10-tetraazacyclododecane-1,4,7,10-tetraacetate). *Z* spectra corresponding to the effects of temperature (A), pH (B), effective agent concentration (C) and TR (D). The CEST effects were generated by a selective continuous-wave square-shaped radiofrequency (RF) saturation pulse duration of 1 s with a B_1 field of 78 μT. In (C), because of 10% D_2O content in each sample, the effective concentration of the EuDOTA–$(gly)_4^-$ agent which contributes to CEST is 90% of the total agent concentration.

too rapid (30). We note that the frequency at which the M/M_0 ratio reaches a minimum, corresponding to the frequency of the bound water signal, is also temperature dependent, with a sensitivity of about −0.22 ppm/°C at 35 °C. However, this broad water signal has an SNR which is an order of magnitude lower than the other nonexchangeable protons (Fig. 1A), thereby reducing the accuracy of temperature determination. The increase in temperature also results in the broadening of both the bound and bulk water peak profiles in the *Z* spectra.

The effect of pH is not as significant as that for temperature with EuDOTA–$(gly)_4^-$. Changing the pH between 6.5 and 8.0 has a small effect on CEST from bound water exchange (Fig. 2B). The relatively minor changes in M/M_0 probably reflect the four pH-dependent −NH protons in the complex that also exchange with solvent protons. This exchange, although not observed directly in the *Z* spectrum, effectively shortens the T_2 value of bulk water (31). Water exchange in PARACEST agents, in general, does not depend on the pH, but other exchangeable functional groups in these complexes may potentially be used as pH-sensitive CEST sites (32).

Changing the concentration of EuDOTA–$(gly)_4^-$ by an order of magnitude produces the largest change in CEST (Fig. 2C). It should be noted that, as a result of the 10% D_2O content in each sample, the actual concentration of the EuDOTA–$(gly)_4^-$ agent which contributes to the CEST effect is only 90% of the total agent concentration. The magnitude of the CEST effect does not increase linearly with concentration at the levels examined here, because we approach maximal CEST (i.e. M/M_0 approaches zero) at agent concentrations greater than 45 mM. These data illustrate that the magnitude of CEST is highly concentration dependent, a problem common to both PARACEST and DIACEST agents for *in vivo* applications (1,2).

The *Z* spectra also exhibit a small dependence on TR, with shorter TR values giving a somewhat larger CEST effect (i.e. smaller M/M_0) (Fig. 2D). During the acquisition of these data, the saturation pulse of 1 s was kept constant and only TR was changed. Although the reason for this observation may not be obvious, this reflects the incomplete relaxation of bulk water protons between scans using a relatively short saturation pulse length (1 s) and a short TR, so that a steady-state level of saturation is achieved that results in a larger net CEST effect. It should also be noted that the bound water exchange resonance in the *Z* spectra at short TR is broader than that at higher TR (Fig. 2D). These data illustrate that one can achieve good CEST contrast without conducting CEST experiments under fully relaxed conditions.

Dual characterization of EuDOTA–$(gly)_4^-$ with BIRDS and CEST imaging

The temperature distributions of a cylindrical glass phantom were examined by BIRDS and CEST imaging with an identical slice location and thickness (Fig. 3). A representative voxel from the CSI grid (Fig. 3A) shows a high SNR for the H4 proton (Fig. 3B), which shifts with a temperature sensitivity of about −0.13 ppm/°C and shows negligible pH dependence (Fig. 1B; Table 1). The absolute temperature in each voxel of the CSI dataset was calculated according to Equation [1] at two different ambient conditions.

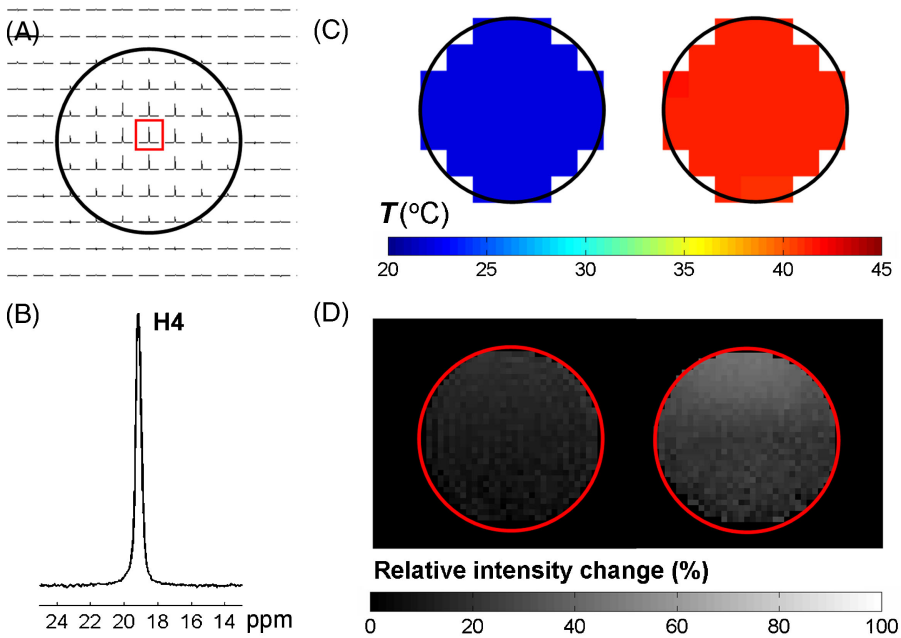

Figure 3. BIRDS (biosensor imaging of redundant deviation in shifts) and CEST (chemical exchange saturation transfer) imaging with europium DOTA–tetraglycinate [EuDOTA–$(gly)_4^-$] ($DOTA^{4-}$, 1,4,7,10-tetraazacyclododecane-1,4,7,10-tetraacetate). *In vitro* temperature effects of a phantom consisting of a cylindrical tube with 20 mM EuDOTA–$(gly)_4^-$ in 10% D_2O at pH 7.0. (A) Proton two-dimensional chemical shift imaging (CSI) dataset demonstrating the distribution of the H4 resonance on a 2-mm slice of the phantom. The CSI voxel dimension was $0.8 \times 0.8 \times 2\,mm^3$. (B) Example of a proton spectrum from a CSI voxel indicated by the red box in (A). (C) *In vitro* BIRDS. Temperature maps of the phantom obtained by BIRDS at room temperature (left) and heated using a water-heating blanket (right). (D) *In vitro* CEST. MRI maps obtained under the same two ambient conditions as above (i.e. left represents room temperature, right represents heating by a water-heating blanket), but each image represents the percentage decrease in intensity caused by the CEST effect calculated according to Equation [3]. A square-shaped radiofrequency (RF) saturation pulse of 1-s duration and a B_1 field of 32.6 μT were used. The CEST contrast is attenuated at the lower temperature as suggested by the *Z* spectra in Fig. 2(A). However, this CEST contrast is not quantitative unless the experimental factors, such as the concentration and pH of EuDOTA–$(gly)_4^-$, as well as TR, are known.

With BIRDS, the average temperature in the phantom was 22.1 ± 0.1 °C with the water bath turned off (Fig. 3C, left) and 41.6 ± 0.1 °C with the water bath turned on (Fig. 3C, right). This agreed well with the temperatures measured using a thermocouple wire (i.e. ~22 °C and ~42 °C for the water bath turned off and on, respectively).

Two spin-echo MRI datasets with CEST contrast were also obtained at these two ambient conditions (Fig. 3D). The change in the intensity of the bulk water signal after presaturation of bound water was calculated relative to the bulk water signal in the absence of saturation, according to Equation [3]. The top halves of the MRI datasets with higher SNR values were used, and regions of poor RF sensitivity further away from the surface coil (i.e. B_1 inhomogeneity) were excluded. With CEST, the results indicate that the average intensity changes in the phantom were $15 \pm 3\%$ (Fig. 3D, left) and $32 \pm 7\%$ (Fig. 3D, right) with the water bath turned off and on, respectively.

To estimate the RF heating of the sample caused by rapid RF pulsing, we repeated both CSI and MRI experiments with a thermocouple wire inserted inside the NMR tube, positioned in the center of the region from which the MR signal was acquired. As a result of high B_0 inhomogeneities induced by the presence of the thermocouple, simultaneous MR data acquisition and temperature measurement by the thermocouple were not possible. The average temperature increase during a 4.5-min-long CSI experiment was 0.024 ± 0.019 °C, whereas, for a 7-min MRI sequence with CEST contrast, the average temperature increase was 0.3 ± 0.1 °C.

DISCUSSION

In this article, we report that EuDOTA–$(gly)_4^-$ possesses dual CEST and BIRDS properties which could potentially improve quantitative biosensing. EuDOTA–$(gly)_4^-$ is a tetraglycinate derivative of the macrocyclic chelate $DOTA^{4-}$, and has been shown to be a PARACEST agent for temperature (5,7,9). The bound water lifetime in EuDOTA–$(gly)^{4-}$ was estimated to be around 300 μs at 298 K (7). However, the CEST efficiency of an agent is given by the product between the bound water lifetime (τ_M) and the chemical shift separation ($\Delta\omega$) between the bound and bulk water peaks (31). EuDOTA–$(gly)_4^-$ has a $\Delta\omega\tau_M$ value in the region of ~7.7 at 1.5 T and ~60 at 11.7 T, where a higher $\Delta\omega\tau_M$ value suggests a more efficient CEST effect (1,2). Thus, LnDOTA–$(gly)_4^-$ is likely to be a more efficient PARACEST agent at higher B_0, although it could still be effective at low B_0 (33), but the CEST efficiency may decrease by nearly an order of magnitude from 11.7 to 1.5 T. These measured CEST properties of EuDOTA–$(gly)_4^-$ are manifested by proton exchange between bulk water and bound water pools (Fig. 1A, inset spectrum), but the H7 amide proton of EuDOTA–$(gly)_4^-$ (Fig. 1A, inset structure) is another exchangeable pool which could be exploited further for additional CEST effects, and remains to be investigated in future studies.

The remaining eight proton signals emanating from the backbone of the $DOTA^{4-}$ chelate (Fig. 1A) do not exchange and therefore are readily detectable by conventional ^1H MRS. Detection by BIRDS is improved if the relaxation properties (Table 1) are exploited to allow short TR experiments with

high-speed CSI. The variation in pH has little effect on the chemical shifts of these protons. The chemical shifts of the protons are sensitive mainly to temperature variations and, amongst all of these protons, H4 is the most sensitive (Table 1). Thus, we propose a second-order dependence between temperature and the H4 chemical shift, as described by Equation [1], because the pH dependence can be ignored within the physiological range (Fig. 1B). This allows temperature measurements with quite high accuracy. For a CSI voxel of $0.8 \times 0.8 \times 2.0\,mm^3$ (as used in this study with SNR in the range 10–30 for the H4 signal), the error in the temperature prediction is less than 0.07 °C (Fig. 1C; Table 2). This level of uncertainty in temperature prediction using EuDOTA–$(gly)_4^-$ with BIRDS compares quite well with other temperature mapping methods, e.g. the *N*-acetyl aspartate–water method or $TmDOTP^{5-}$ with BIRDS (23). However, we used only one proton resonance of EuDOTA–$(gly)_4^-$ (i.e. H4; see Table 1) for temperature prediction. If some of the other proton resonances of EuDOTA–$(gly)_4^-$ (e.g. H5 and H6, both of which have comparable temperature sensitivities, see Table 1) are also used—as with $TmDOTP^{5-}$, where three proton resonances are employed (23)—the redundancy of information contained within the biosensor could be improved to reduce the uncertainty in temperature even further. We envisage that the uncertainty in temperature prediction using EuDOTA–$(gly)_4^-$ with three proton resonances (i.e. H4–H6; see Table 1) may compare quite well with the temperature sensitivity of $TmDOTMA^-$ with BIRDS (24).

The CEST contrast is based on the transfer of magnetization via proton exchange from the exchangeable solute pool to the bulk water pool, and the effect can be observed if the system is in 'slow exchange' or $\Delta\omega\tau_M \geq 1$. Therefore, an agent with a relatively large $\Delta\omega$ value is better because it provides a CEST effect even with a short τ_M. In addition, as pointed out earlier, the much larger chemical shift separation between signals arising from the pools of exchangeable protons from PARACEST agents (*versus* DIACEST agents) reduces the vulnerability of CEST contrast to B_0 inhomogeneity (i.e. poor shim). However, for the CEST effect of EuDOTA–$(gly)^{4-}$ to be easily quantifiable, the MRI contrast needs to respond specifically to temperature (Fig. 2A) and not to other experimental factors (Fig. 2B–D). A primary concern for quantitative CEST contrast is the dependence of the effect on agent concentration (Fig. 2C). Although pH and TR effects on the M/M_0 ratio for EuDOTA–$(gly)^{4-}$ are small (Fig. 2B, D), they may not be ignored with other PARACEST agents. Another issue of concern for CEST contrast that requires further study is B_1 inhomogeneity (e.g. with RF surface coil), as observed in the CEST imaging data (Fig. 3D).

In vitro CEST imaging showed ~15% and ~30% contrast in the MRI data with the water bath turned off (Fig. 3D, left) and on (Fig. 3D, right), which correspond to ~22 °C (Fig. 3C, left) and ~42 °C (Fig. 3C, right), respectively, measured by BIRDS and thermocouple wires. However, additional information is needed to convert the qualitative MRI intensity change from CEST imaging to actual temperature values. First and foremost, it is obligatory to know the concentration of EuDOTA–$(gly)_4^-$. In addition, it is also necessary to negate any effects on the MRI intensity change caused by contributions from B_0 inhomogeneity, B_1 inhomogeneity, TR and/or pH. Although, in this study, we have shown the effect of TR and pH on CEST quantification with EuDOTA–$(gly)_4^-$, the experimental conditions were not ideal for examining the effects of B_0 and B_1 inhomogeneities, because we used ideal B_0 shim conditions and an RF surface coil with small SNR variations. Future studies need to assess quantitatively the impact of B_0 and B_1 inhomogeneities on the CEST effect with EuDOTA–$(gly)_4^-$.

Based primarily on information obtained from $TmDOTP^{5-}$ and $TmDOTMA^-$, BIRDS quantification is not as susceptible to many of these experimental factors (23,24). Physiological information extracted from CSI data, and thus BIRDS, is inherently independent of the agent concentration (i.e. beyond the detection limit). As physiological quantification is dependent on the nonexchangeable resonance chemical shifts, and not intensity, inherent B_1 inhomogeneity present in MRI or MRS data with RF surface coils is much less of a concern for BIRDS. Furthermore, physiological quantification (e.g. temperature, pH, etc.) based on shifts of the nonexchangeable protons is nearly constant across different B_0 values, thus enabling BIRDS properties to be nearly independent of B_0. Because the T_2/T_1 ratios of these protons are only slightly varying across different B_0 values, at nominal TR values only marginal SNR loss is expected at a lower *versus* higher B_0. Indeed, for some agent designs, it is even possible to reach T_2/T_1 ratios of close to unity, thus allowing optimal sensitivity of detection, as SNR is directly proportional to $\sqrt{T_2/T_1}$. The extremely short T_2 values of the nonexchangeable protons make their detection, and thus BIRDS, nearly impervious to B_0 inhomogeneity. Furthermore, BIRDS can easily measure the ambient conditions of the agent (i.e. temperature and/or pH). All of these benefits from BIRDS could be used to improve quantitative imaging with CEST. For example, BIRDS can be used to measure the distribution of both sample temperature and agent concentration. Using these measurements, the CEST experiment may be corrected for temperature and/or agent concentration effects to accurately measure another physiological parameter, such as pH. Recently, a new MRI-based method proposed by Dixon *et al*. (30) has been reported, which quantifies the CEST effect of a PARACEST agent with multiparametric modeling, thereby negating the need for the agent's concentration. It would be extremely important to compare the accuracies of dual biosensing with BIRDS–CEST *versus* the method of Dixon *et al*. for molecular imaging applications.

Another advantage of EuDOTA–$(gly)_4^-$ is that it has the potential for translation to *in vivo* studies. Pharmacokinetics studies on rats injected with 100 μL of a solution of EuDOTA–$(gly)_4^-$ containing traces of radioactive lutetium(III) ion ($^{177}Lu^{3+}$), in the form of ^{177}LuDOTA–$(gly)_4^-$, indicated an average elimination half-life of 20 min (15). Biodistribution measurements showed that, 30 min after injection, the residual ^{177}LuDOTA–$(gly)_4^-$ was localized mainly in blood, kidney and urine, whereas, 2 h later, the ^{177}LuDOTA–$(gly)_4^-$ levels had decreased significantly as a result of rapid excretion. Toxicity studies of EuDOTA–$(gly)_4^-$ showed that a relatively high dose (1 mmol/kg) was well tolerated, with a minimal effect on the health of the animal. Although EuDOTA–$(gly)_4^-$ has a relatively low thermodynamic stability compared with other agents containing the gadolinium(III) ion (i.e. Gd^{3+}), e.g. GdDOTA (Dotarem), it exhibits a relatively high kinetic stability, which represents the major factor in determining the toxicity of any Ln^{3+}-based agent. However, *in vivo* studies with EuDOTA–$(gly)_4^-$ may require that the agent remain in circulation for several hours during the accumulation of MR data, perhaps aided by renal ligation (22–24). In that case, additional toxicity measurements, coupled with SNR estimation *in vivo* under renal ligation conditions, will be required to correctly estimate the optimal *in vivo* dose needed for EuDOTA–$(gly)_4^-$ in rats, as performed previously for $TmDOTP^{5-}$

and $TmDOTMA^{-}$ (23,24). Moreover, the use of relatively high saturation powers during CEST experiments may result in slight heating of the sample investigated. Although the temperature increase observed during the CEST experiment in this study was quite small ($< 0.3\,^{\circ}C$), special attention needs to be employed during eventual preclinical and clinical applications using CEST imaging. A further issue for preclinical and clinical applications will be the exclusion of B_0 and B_1 inhomogeneities on the CEST effect. For the latter concern, however, BIRDS could be used to potentially circumvent these problems, because it is less affected by B_0 and B_1 inhomogeneities.

CONCLUSIONS

Using EuDOTA–$(gly)_4^-$, we obtained *in vitro* temperature data (measured by BIRDS) at two different ambient conditions within $0.1\,^{\circ}C$ accuracy of the actual temperature of the phantom (measured by a thermocouple). Quantitative information from BIRDS obtained at CSI spatial resolution (i.e. voxel size of $0.8 \times 0.8 \times 2.0\,mm^3$) may be used to improve the qualitative CEST contrast, which shows higher MRI spatial resolution (i.e. voxel size of $0.125 \times 0.125 \times 2.0\,mm^3$) but may suffer from unknown contributions from various experimental factors. These results suggest that EuDOTA–$(gly)_4^-$ and other PARACEST-like agents, which possess large numbers of exchangeable and non-exchangeable protons, can be used as a dual biosensor featuring both CEST and BIRDS properties. Future studies should seek agent designs that enhance BIRDS sensitivity without diminishing the advantages of CEST, as these combined properties in a single molecular probe could have a wide range of MRI and MRS applications in functional brain studies (34–38).

Acknowledgements

The authors thank the scientists and engineers at the Magnetic Resonance Research Center (MRRC) (mrrc.yale.edu) and Core Center for Quantitative Neuroscience with Magnetic Resonance (QNMR) (qnmr.yale.edu). This work was supported by grants from the National Institutes of Health (R01 MH-067528 to FH, R01 CA-140102 to FH/GEK, R01 EB-011968 to FH, R01 AG-034953 to DLR, P30 NS-52519 to FH, R01 CA-115531 to ADS, R01 EB-004582 to ADS and P41 RR-002584 to ADS).

REFERENCES

1. Zhou J, van Zijl PC. Chemical exchange saturation transfer imaging and spectroscopy. Prog. Nucl. Magn. Reson. Spectrosc. 2006; 48: 109–136.
2. Sherry AD, Woods M. Chemical exchange saturation transfer contrast agents for magnetic resonance imaging. Annu. Rev. Biomed. Eng. 2008; 10: 391–411.
3. Ward KM, Aletras AH, Balaban RS. A new class of contrast agents for MRI based on proton chemical exchange dependent saturation transfer (CEST). J. Magn. Reson. 2000; 143(1): 79–87.
4. Zhang S, Wu K, Sherry AD. Unusually sharp dependence of water exchange rate versus lanthanide ionic radii for a series of tetraamide complexes. J. Am. Chem. Soc. 2002; 124(16): 4226–4227.
5. Aime S, Barge A, Delli Castelli D, Fedeli F, Mortillaro A, Nielsen FU, Terreno E. Paramagnetic lanthanide(III) complexes as pH-sensitive chemical exchange saturation transfer (CEST) contrast agents for MRI applications. Magn. Reson. Med. 2002; 47(4): 639–648.
6. Aime S, Barge A, Gianolio E, Pagliarin R, Silengo L, Tei L. High relaxivity contrast agents for MRI and molecular imaging. Ernst Schering Res. Found. Workshop, 2005; 49: 99–121.
7. Zhang S, Sherry AD. Physical characteristics of lanthanide complexes that act as magnetization transfer (MT) contrast agents. J. Solid State Chem. 2003; 171(1–2): 38–43.
8. Li AX, Wojciechowski F, Suchy M, Jones CK, Hudson RH, Menon RS, Bartha R. A sensitive PARACEST contrast agent for temperature MRI: Eu^{3+}-DOTAM-glycine (Gly)-phenylalanine (Phe). Magn. Reson. Med. 2008; 59(2): 374–381.
9. Zhang S, Malloy CR, Sherry AD. MRI thermometry based on PARACEST agents. J. Am. Chem. Soc. 2005; 127(50): 17 572–17 573.
10. Aime S, Delli Castelli D, Fedeli F, Terreno E. A paramagnetic MRI-CEST agent responsive to lactate concentration. J. Am. Chem. Soc. 2002; 124(32): 9364–9365.
11. Zhang S, Trokowski R, Sherry AD. A paramagnetic CEST agent for imaging glucose by MRI. J. Am. Chem. Soc. 2003; 125(50): 15 288–15 289.
12. Ren J, Trokowski R, Zhang S, Malloy CR, Sherry AD. Imaging the tissue distribution of glucose in livers using a PARACEST sensor. Magn. Reson. Med. 2008; 60(5): 1047–1055.
13. Dhingra K, Maier ME, Beyerlein M, Angelovski G, Logothetis NK. Synthesis and characterization of a smart contrast agent sensitive to calcium. Chem. Commun. (Camb.) 2008; 7(29): 3444–3446.
14. Esqueda AC, Lopez JA, Andreu-de-Riquer G, Alvarado-Monzon JC, Ratnakar J, Lubag AJ, Sherry AD, De Leon-Rodriguez LM. A new gadolinium-based MRI zinc sensor. J. Am. Chem. Soc. 2009; 131(32): 11 387–11 391.
15. Sherry AD, Caravan P, Lenkinski RE. Primer on gadolinium chemistry. J. Magn. Reson. Imaging, 2009; 30(6): 1240–1248.
16. Aime S, Botta M, Fasano M, Marques MP, Geraldes CF, Pubanz D, Merbach AE. Conformational and coordination equilibria on DOTA complexes of lanthanide metal ions in aqueous solution studied by (1)H-NMR spectroscopy. Inorg. Chem. 1997; 36(10): 2059–2068.
17. Geraldes CFGC, Sherry AD, Kiefer GE. The solution structure of Ln $(DOTP)^{5-}$ complexes. A comparison of lanthanide-induced paramagnetic shifts with the MMX energy-minimized structure. J. Magn. Reson. 1992; 97(2): 290–304.
18. Sherry AD, Ren J, Huskens J, Brucher E, Toth E, Geraldes CFCG, Castro MMCA, Cacheris WP. Characterization of lanthanide(III) DOTP complexes: thermodynamics, protonation, and coordination to alkali metal ions. Inorg. Chem. 1996; 35(16): 4604–4612.
19. Pasha A, Lin M, Tircso G, Rostollan CL, Woods M, Kiefer GE, Sherry AD, Sun X. Synthesis and evaluation of lanthanide ion DOTA–tetraamide complexes bearing peripheral hydroxyl groups. J. Biol. Inorg. Chem. 2009; 14(3): 421–438.
20. Zuo CS, Bowers JL, Metz KR, Nosaka T, Sherry AD, Clouse ME. $TmDOTP^{5-}$: a substance for NMR temperature measurements in vivo. Magn. Reson. Med. 1996; 36(6): 955–959.
21. Bansal N, Germann MJ, Lazar I, Malloy CR, Sherry AD. In vivo Na-23 MR imaging and spectroscopy of rat brain during $TmDOTP^{5-}$ infusion. J. Magn. Reson. Imaging, 1992; 2(4): 385–391.
22. Trubel HK, Maciejewski PK, Farber JH, Hyder F. Brain temperature measured by ^{1}H-NMR in conjunction with a lanthanide complex. J. Appl. Physiol. 2003; 94(4): 1641–1649.
23. Coman D, Trubel HK, Rycyna RE, Hyder F. Brain temperature and pH measured by (1)H chemical shift imaging of a thulium agent. NMR Biomed. 2009; 22(2): 229–239.
24. Coman D, Trubel HK, Hyder F. Brain temperature by Biosensor Imaging of Redundant Deviation in Shifts (BIRDS): comparison between $TmDOTP^{5-}$ and $TmDOTMA^{-}$. NMR Biomed. 2010; 23(3): 277–285.
25. Findeisen M, Brand T, Berger S. A ^{1}H-NMR thermometer suitable for cryoprobes. Magn. Reson. Chem. 2007; 45(2): 175–178.
26. Morton DW, Maravilla KR, Meno JR, Winn HR. Clinically relevant rat model for testing BOLD functional MR imaging techniques by using single-shot echo-planar imaging at 1.5 T. Radiology, 2001; 218(2): 598–601.
27. Grad J, Bryant RG. Nuclear magnetic cross-relaxation spectroscopy. J. Magn. Reson. 1990; 90(1): 1–8.
28. Grad J, Mendelson D, Hyder F, Bryant RG. Applications of nuclear magnetic cross-relaxation spectroscopy to tissues. Magn. Reson. Med. 1991; 17(2): 452–459.
29. Bevington PR. *Data Reduction and Error Analysis for the Physical Sciences*. McGraw-Hill: New York, NY, 1969.

30. Dixon WT, Ren J, Lubag AJ, Ratnakar J, Vinogradov E, Hancu I, Lenkinski RE, Sherry AD. A concentration-independent method to measure exchange rates in PARACEST agents. Magn. Reson. Med. 2010; 63(3): 625–632.
31. Zhang S, Merritt M, Woessner DE, Lenkinski RE, Sherry AD. PARACEST agents: modulating MRI contrast via water proton exchange. Acc. Chem. Res. 2003; 36(10): 783–790.
32. Pikkemaat JA, Wegh RT, Lamerichs R, van de Molengraaf RA, Langereis S, Burdinski D, Raymond AY, Janssen HM, de Waal BF, Willard NP, Meijer EW, Grull H. Dendritic PARACEST contrast agents for magnetic resonance imaging. Contrast Media Mol. Imaging, 2007; 2(5): 229–239.
33. Vinogradov E, He H, Lubag A, Balschi JA, Sherry AD, Lenkinski RE. MRI detection of paramagnetic chemical exchange effects in mice kidneys in vivo. Magn. Reson. Med. 2007; 58(4): 650–655.
34. Trubel H, Herman P, Kampmann C, Novotny E, Hyder F. [Selective pharyngeal brain cooling]. Biomed. Tech. (Berl.) 2003; 48(11): 298–300.
35. Trubel H, Herman P, Kampmann C, Huth R, Maciejewski PK, Novotny E, Hyder F. A novel approach for selective brain cooling: implications for hypercapnia and seizure activity. Intensive Care Med. 2004; 30(9): 1829–1833.
36. Trubel H, Herman P, Kampmann C, Novotny E, Hyder F. [Duration of induced seizures during selective pharyngeal brain cooling]. Biomed. Tech. (Berl.) 2004; 49(10): 279–281.
37. Trubel HK, Sacolick LI, Hyder F. Regional temperature changes in the brain during somatosensory stimulation. J. Cereb. Blood Flow Metab. 2006; 26(1): 68–78.
38. Maandag NJ, Coman D, Sanganahalli BG, Herman P, Smith AJ, Blumenfeld H, Shulman RG, Hyder F. Energetics of neuronal signaling and fMRI activity. Proc. Natl. Acad. Sci. USA, 2007; 104(51): 20 546–20 551.